

CONSTRAINING PARAMETERS OF WHITE-DWARF BINARIES USING GRAVITATIONAL-WAVE AND ELECTROMAGNETIC OBSERVATIONS

SWETA SHAH^{1,2} AND GIJS NELEMANS^{1,2,3}

¹Department of Astrophysics/ IMAPP, Radboud University Nijmegen, P.O. Box 9010, 6500 GL Nijmegen, The Netherlands

²Nikhef National Institute for Subatomic Physics, Science Park 105, 1098 XG Amsterdam, The Netherlands

³Institute for Astronomy, KU Leuven, Celestijnenlaan 200D, 3001 Leuven, Belgium

(Dated: June 16, 2014)

ABSTRACT

The space-based gravitational wave (GW) detector, *evolved Laser Interferometer Space Antenna* (eLISA) is expected to observe millions of compact Galactic binaries that populate our Milky Way. GW measurements obtained from the eLISA detector are in many cases complimentary to possible electro-magnetic (EM) data. In our previous papers, we have shown that the EM data can significantly enhance our knowledge of the astrophysically relevant GW parameters of the Galactic binaries, such as the amplitude and inclination. This is possible due to the presence of some strong correlations between GW parameters that are measurable by both EM and GW observations, for example the inclination and sky position. In this paper, we quantify the constraints in the physical parameters of the white-dwarf binaries, i.e. the individual masses, chirp mass and the distance to the source that can be obtained by combining the full set of EM measurements such as the inclination, radial velocities, distances and/or individual masses with the GW measurements. We find the following $2 - \sigma$ fractional uncertainties in the parameters of interest. The EM observations of distance constrains the chirp mass to $\sim 15 - 25\%$, whereas EM data of a single-lined spectroscopic binary constrains the secondary mass and the distance with factors of 2 to $\sim 40\%$. The single-line spectroscopic data complemented with distance constrains the secondary mass to $\sim 25 - 30\%$. Finally EM data on double-lined spectroscopic binary constrains the distance to $\sim 30\%$. All of these constraints depend on the inclination and the signal strength of the binary systems. We also find that the EM information on distance and/or the radial velocity are the most useful in improving the estimate of the secondary mass, inclination and/or distance.

Subject headings: stars: binaries - gravitational waves, Galactic binaries - GW parameters, GW detectors - LISA

1. INTRODUCTION

Gravitational wave (GW) observations and electromagnetic (EM) observations can be used to study compact Galactic binaries independently and often these two ways provide different measurements of the same system. There are about ~ 50 of these binaries that have been studied in the optical, UV, and X-ray wavelengths (e.g. Roelofs et al. 2010). This number is expected to grow by a factor of ~ 100 (Nissanke et al. 2012) when a space-based gravitational wave (GW) observatory like the recently eLISA¹ will be in operation. This detector is expected to observe millions of compact Galactic binaries with periods shorter than about a few hours (Nelemans 2009; Amaro-Seoane et al. 2013), amongst other astrophysical sources. Of those millions of binaries we will be able to resolve several thousands. It has been shown (Shah et al. 2012, Paper I, hereafter) that for a non-eclipsing binary system (for example AM CVn), its EM measurement of the inclination, ι can improve the error on the GW amplitude (\mathcal{A}) significantly depending on the strength of the GW signal and the magnitude of the EM uncertainty in the inclination. \mathcal{A} is a GW parameter which is given by a combination of the masses,

orbital period and distance to the source:

$$\mathcal{A} = \frac{4(G\mathcal{M}_c)^{5/3}}{c^4 d} (\pi f)^{2/3}, \quad (1)$$

where, d is the distance to the source, f is the source's GW frequency ($2/P_{\text{orb}}$), and \mathcal{M}_c is the chirp mass defined as:

$$\mathcal{M}_c \equiv (m_1 m_2)^{3/5} / (m_1 + m_2)^{1/5}. \quad (2)$$

From the GW observations alone, one typically cannot measure the individual masses or the distance since they are degenerate via Eqs. 1, 2. In the rare cases that a precise orbital decay (\dot{f}), can be measured from GW data then the distance can be estimated (with the assumption that the frequency evolution is dictated by GW radiation only) by determining \mathcal{M}_c from the measured f and \dot{f} via the equation (Peters & Mathews 1963):

$$\dot{f} = \frac{96 \pi G^{5/3}}{5 c^5} (\pi \mathcal{M}_c)^{5/3} f^{11/3}. \quad (3)$$

For the compact binaries that have been observed with the optical telescopes, a subset of which will also be detected by eLISA, their EM data often provide measurements of the orbital period P_{orb} , the primary mass (m_1), sometimes the secondary mass (m_2), the distance (d) and the radial velocity amplitude (K_i). We use these measurements for a few binaries to show the quantitative

s.shah@astro.ru.nl

¹ In preparation by ESA, expected launch in ~ 2034

improvements in their GW and other physical parameters. Many of these binaries can/could still be found electromagnetically before or after eLISA discoveries.

We have previously shown that knowing sky positions from EM data can improve the GW uncertainties on \mathcal{A} and ι depending on the particular geometry and orientation of the binary systems (Shah et al. 2013). Thus, so far we have quantitatively studied the improvement factors in the uncertainties of the parameters that can be gained from *prior* knowledge of parameters which are common to both GW and EM observations, for example inclination, and sky position.

In this paper we go beyond constraining *only* those GW parameters which are *also* measured independently from the EM data. We explore various combinations of *any* possible EM observations and the GW measurements in constraining the *useful parameters* of the binaries that are astro-physically interesting, for example the individual masses. Because their GW signal is significantly affected we consider high-inclination (sometimes eclipsing) and (low inclination) binary systems. We review the GW data analysis methods in Sect. 2. In Sect. 3, we explore the information gained by combining EM measurements in different ways where the EM data can be the radial velocity of one of the binary components, K_i , m_1 , m_2 , d , and P_{orb} . Specifically, we classify various combinations into a number of scenarios in discussing the parameter constraints.

2. PARAMETER UNCERTAINTIES FROM GW OBSERVATIONS

For our analyses below, we consider one of the eLISA *verification binaries* J065133.33+284423.3 (J0651, hereafter; Brown et al. (2011)). We also consider a second (hypothetical) system with higher masses which we will refer to as “the high mass binary”. Their GW parameter values are listed in Table 1. Before looking at the EM data we briefly recap out GW data analysis method. We have used Fisher matrix studies (e.g Cutler 1998) to extract the GW parameter uncertainties and correlations in the GW parameters that describe the compact binary sources. Our method and application of Fisher information matrix (FIM) for eLISA binaries together with their signal modeling and the noise from the detector and the Galactic foreground have been described in detail in Paper I. Most of the binaries will be monochromatic sources and such sources are completely characterized by a set of seven parameters, dimensionless amplitude (\mathcal{A}), frequency (f), polarization angle (ψ), initial GW phase (ϕ_0), inclination ($\cos \iota$), ecliptic latitude ($\sin \beta$), and ecliptic longitude (λ). From the GW signal of a binary and a Gaussian noise we can use FIM to estimate the parameter uncertainties. The inverse of the FIM is the variance-covariance matrix whose diagonal elements are the GW uncertainties and the off-diagonal elements are the correlations between the two parameters. We do the GW analyses of the above mentioned binaries for eLISA observations of two years. We note that Fisher-based method is a quick way of computing parameter uncertainties and their correlations in which these uncertainties are estimated locally at the true parameter values and therefore by definition the method cannot be used to sample the entire posterior distribution of the parameters. Additionally Fisher-based results

hold in the limit of strong signals with a Gaussian noise (e.g. Vallisneri 2008, see also Appendix).

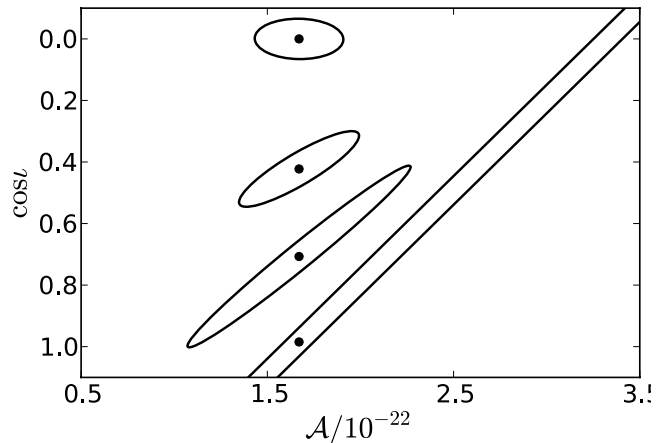


FIG. 1.— Two-dimensional error ellipses of \mathcal{A} and $\cos \iota$ extracted from the variance-covariance matrix for J0651 binary system with varying orientation in its ι . The distributions with larger to smaller ellipses correspond to $\iota = 10^\circ, 45^\circ, 65^\circ, 90^\circ$ respectively. The black dots are the GW parameter values (see Table 1) about which the FIM is evaluated for the corresponding orientations.

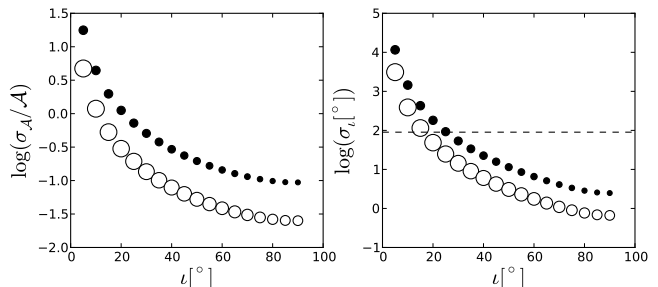


FIG. 2.— GW uncertainties in amplitude and inclination for J0651 as a function of inclination calculated from Fisher matrices. Filled circles are for J0651 with $m_1, m_2 = 0.25, 0.55 M_\odot$ and open circles are for the case of the high mass binary with $m_1, m_2 = 0.8, 0.8 M_\odot$. The size of the marker represents the S/N at each inclination. The dashed line on the right-panel marks the unphysical values for the inclination (see text).

The two-dimensional GW distribution in amplitude and inclination given by the variance-covariance matrix for J0651 parameters are shown in Figure 1 for a number of inclinations. The largest and most highly correlated distribution is that with $\iota = 10^\circ$ and the weakest correlation is that with $\iota = 90^\circ$. The behavior of these distributions reflect the strength of the correlation between amplitude and inclination. As discussed in Paper I, the low inclination systems $\iota \leq 45^\circ$ have very similar signal shapes, whereas systems with high inclinations are distinguishable by both the shape and structure for small differences in inclinations. Thus, for low-inclination binaries a small change in ι is indistinguishable from a small change in its \mathcal{A} . On the other hand for high-inclination binaries a small change in inclination produces a noticeably different signal explaining the uncertainties in \mathcal{A} and ι becoming large to small with increasing inclination. The GW uncertainties for the amplitude and inclination as a function of inclination are shown in Figure 2 for J0651 (in filled circles) and the high mass binary (in open

TABLE 1
 GW PARAMETER VALUES OF J0651

	\mathcal{A} [$\times 10^{-22}$]	\mathcal{M}_c [M_\odot]	ϕ_0 [rad]	$\cos \iota$	f [$\times 10^{-3}$] [Hz]	ψ [rad]	$\sin \beta$	λ [rad]	S/N
J0651	1.67 ^a , 6.71 ^b	0.32 ^a , 0.70 ^b	π	0.007	2.61	$\pi/2$	0.101	1.77	$\sim 13^a, 50^b$

^a for $m_1 = 0.25M_\odot$, $m_2 = 0.55M_\odot$, $d = 1.0$ kpc ^b for $m_1 = 0.8M_\odot$, $m_2 = 0.8M_\odot$, $d = 1.0$ kpc

circles). The strong increase in uncertainty trends for low inclination systems is due to the correlation between amplitude and inclination (Shah et al. 2012). Clearly the high mass binary has larger S/N which gives smaller uncertainties in both of its parameters shown in open circles in the figure compared to that of J0651. Observe that inclination is a cyclic parameter and is bounded between $0^\circ \leq \iota \leq 90^\circ$ and yet we get very large uncertainties from Fisher matrix for lower inclinations systems shown in the right panel of in Figure 1. This is due to the fact that Fisher matrix methods are based on the linearised signal approximation as a result of which it is not sensitive to the bounded parameters that describe the signal model (Vallisneri 2008). In other words in FIM one computes the uncertainties in parameters based on variation of the signal with respect to the parameters at the true parameter values and the fact that far away from the true value the parameter has a bound is not taken into account by the FIM. When the uncertainty in a bounded parameter exceeds its physically allowed range, it means the quantity cannot be determined from GW data analysis. The dashed line in in Figure 2 indicates the value (at 90°) beyond which the uncertainties in ι imply unphysical values for the inclination. Since the low inclination systems on the left-side of the plot are affected by this, corrections have to be applied to the corresponding (over-estimated) uncertainties in amplitude in the left panel by discarding the unphysical range in the inclination (Shah et al. 2013). One way to correct these unphysical values is by taking a rectangular prior on the inclination. This in effect will cut off the posterior distribution in the parameters at the physical bounds described by the prior. Note that cutting off the error ellipses at lower inclinations in Figure 1 is reasonable because taking strict bounds far away from the real value about which Fisher uncertainties are computed will not change the shape and slope significantly. The cut off in the posterior distributions due to rectangular priors will skew the means of the parameter distributions away from the real value (Rodriguez et al. 2013, Eq. C4). Furthermore we stress the fact that the Fisher matrix method is an *estimate* and cannot, follow the posterior in detail (see Appendix).

The normalized correlations between all the seven parameters for an eclipsing and non-eclipsing orientations of J0651 are listed in the variance-covariance matrices (VCM) in the Appendix. We will make use of these parameter uncertainties and their corresponding correlations when combining with various EM data in Sect. 3.

2.1. GW information only

We start by considering the case where we only have the GW data. From the GW observations, the astrophysical parameters of interest for a monochromatic source are its f , \mathcal{A} and ι . From the GW data analysis the frequency of the source will be very well determined, $\sigma_f/f \sim 10^{-6}$ Hz (e.g. Paper I) for a 10^{-3} Hz source,

so we consider that f is essentially known with a fixed value. Given that most of the binaries that we will observe with eLISA will be binary white-dwarfs (WD) (Nelemans et al. 2001), we can restrict their masses to $m_i \in [0.1, 1.4] M_\odot$. For simplicity we take *uniform* distributions for both masses in this range. This provides a distribution in the system's chirp mass, which will provide an upper limit on the distance for the source. In Figure 3 we show these estimates in d with their 95 percentile (or $2-\sigma$ uncertainties) as a function of inclination for both J0651 (in black) and for the high mass binary with equal high-mass components (in grey). The dashed line (in black) is the real value of the distance for both systems. The lower medians of distances at the lower inclinations for both systems are explained by the fact that at $\iota = 5^\circ$, the GW distribution of \mathcal{A} has a long uniform tail. This is shown in Figure 4 where we compare the distributions of \mathcal{A} for two inclinations: 5° (in black), and 90° (in grey) in the left panel. For a fixed distribution of \mathcal{M}_c , the corresponding distributions in d are shown in the right panel where the solid vertical lines are the distribution medians and dashed vertical line is the real value. We can see that $\mathcal{A}_{\text{median}}^{5^\circ} > \mathcal{A}_{\text{median}}^{90^\circ}$ thus giving $d_{\text{median}}^{5^\circ} < d_{\text{median}}^{90^\circ}$ via Eq. 1 for a fixed \mathcal{M}_c . Also, observe

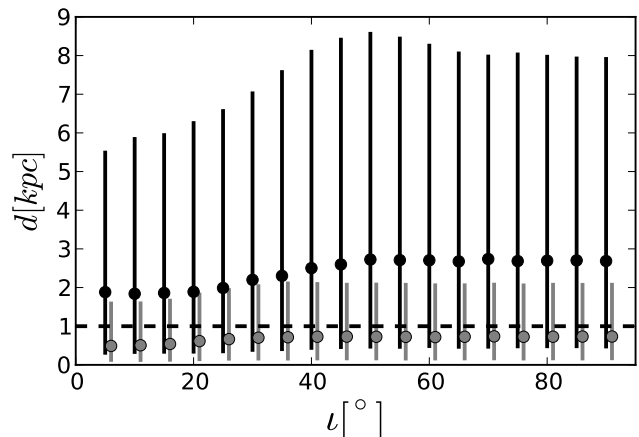


FIG. 3.— *GW data only*: 95 percentile in distance assuming finite chirp mass for J0651 in black lines and the high mass binary in grey lines. The dashed line (in black) is the true value. For clarity the constraints for the high mass binary are shifted to the right. We do this for all the cases below.

that the median distances are over-estimated for J0651 for all inclinations and this is because the real value of the median in \mathcal{M}_c is much smaller than that computed from uniform distributions in m_i , which is the same for all inclinations. Whereas for the high mass binary the computed median in \mathcal{M}_c is close to its real value thus translating into smaller offsets in the median distances in Figure 3. In the figure, the 95 percentiles in the distance slightly increase as a function of inclination even though the uncertainties in \mathcal{A} has the opposite behavior (see Figure 2). This is because the \mathcal{M}_c has a very large

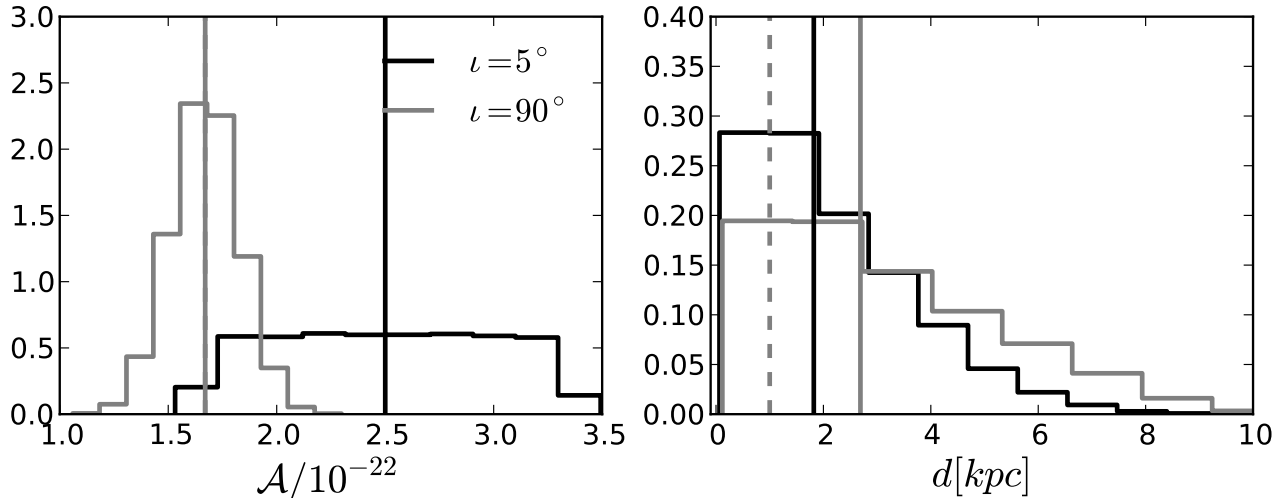


FIG. 4.— *GW data only*: Left: Example of 1D distributions in \mathcal{A} from GW data for two inclinations as labeled and their corresponding distributions. Right: Assuming a finite \mathcal{M}_c , this gives corresponding distributions in distance. The solid lines (in grey and black) are the medians of the distributions whereas the dashed line (over-plotted on thick black solid line) is the real value of the parameters. Note that in the left panel the real value is the same as the median of the grey distribution and thus they overlap.

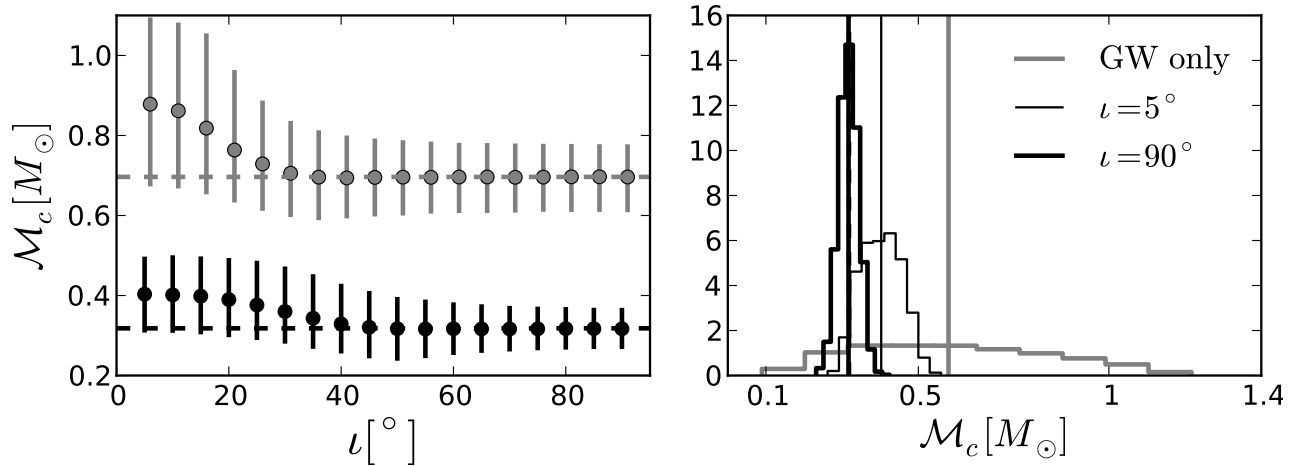


FIG. 5.— *Scenario 1 (known distance)*: Left: 95 percentile in chirp mass given GW data on \mathcal{A} and EM data on distance for J0651 (in black) and high mass binary (in grey). Right: Example of 1D distributions in the \mathcal{M}_c for two inclinations as labeled for the J0651. The solid lines are the medians of the distributions whereas the dashed line (over-plotted on thick black solid line) is the real value of the \mathcal{M}_c . For comparison, the \mathcal{M}_c computed from uniform distribution of masses is shown in grey.

fractional uncertainty compared to that of the \mathcal{A} and thus the relative error uncertainties in the chirp mass dominates those in the distance, which remain roughly constant for all inclinations.

3. COMBINING EM & GW OBSERVATIONS

In all the various scenarios we analyze below, we take the EM parameters with an uncertainty of 10% which is inspired by observational uncertainties of J0651. This binary is a well known EM source and also a guaranteed source for eLISA. J0651 is an eclipsing system and such an orientation of a nearby binary allows accurate EM measurements of its orbital parameters, and the masses (accuracies of $\sim 15\%$ (primary mass); 8% (secondary mass)) from observing the spectra, radial velocities and eclipses of each star by the other (Brown et al. 2011). Furthermore its rate of change of orbital period has also been measured from follow-up high speed photometry from ~ 1 yr. worth of data to an accuracy of $\sim 30\%$ (Hermes et al. 2012), and this will improve in the course of time. In this section we classify specific (possible) sce-

narios where we could have one or more EM data on the white dwarf binary parameters. We explicitly state how much the knowledge of any of the various parameters that describe the *physical* properties of a binary system can be further improved if we can fold in various combinations of the existing EM and/or GW observations. We construct three specific scenarios below based on the typical knowledge from the EM observations:

- EM data on distance
- Single-line spectroscopic data (complemented with or without the distance measurement)
- Double-line spectroscopic data

In all the scenarios the GW information on amplitude, inclination and frequency from Sect. 2.1 are used.

3.1. Scenario 1: EM observation of the distance

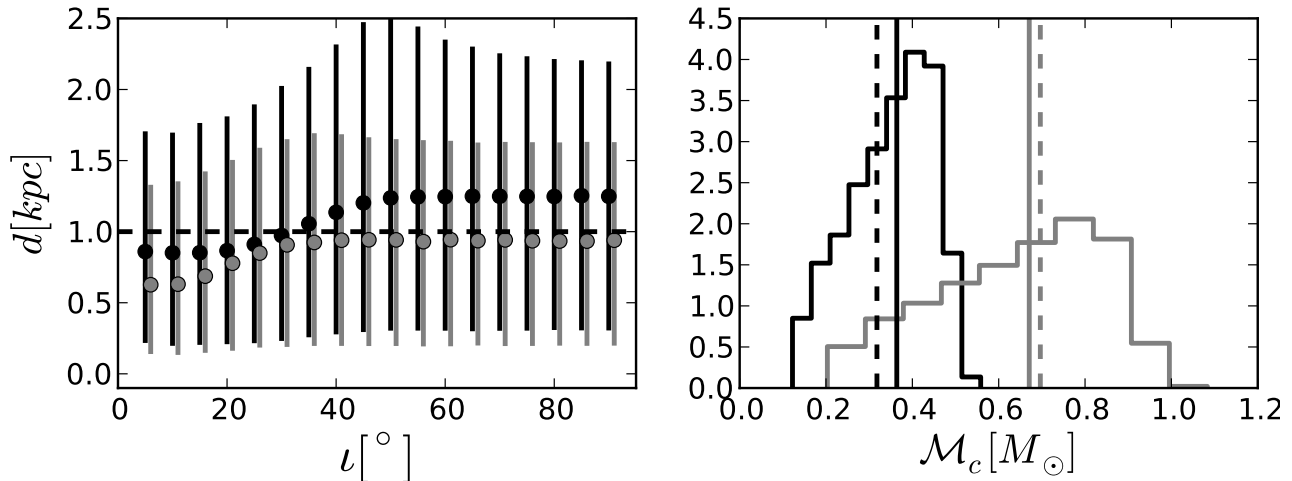


FIG. 6.— *Scenario 2a*: Left: 95 percentile in the distance given GW data on \mathcal{A} and EM data on m_1 for J0651 (in black) and the high mass binary (in grey). Note that \mathcal{M}_c distribution is same at all inclinations for each binary. Right: Comparison of \mathcal{M}_c for J0651 (in black) and for the high mass system (in grey) where solid lines are the medians of the distributions and dashed lines are the real values.

Measuring distances accurately is made feasible by the *Gaia* mission (de Bruijne 2012), a new astrometric satellite. *Gaia* is expected to measure stellar parallaxes of millions of stars with μarcsec accuracy depending on how bright a star is. For example at 1 kpc, J0651 ($g = 19.1$ mag) would have a $\sim 300\mu\text{arcsec}$ accuracy in the parallax measurement corresponding to a fractional accuracy in distance of $\sim 10\%$ (e.g. Bailer-Jones 2009). There is also some indication of the distance of the binary from its absolute magnitude. The uncertainties in d from such measurements are also of the order of several percent or 10% for the case of J0651 (Brown et al. 2011).

A sole EM measurement of the distance of a WD binary might be possible in cases where the system is identified as a WD binary but it is too faint to measure other parameters. For instance from the wide-field surveys it is often possible to identify WD from their colors (Verbeek et al. 2013). Given the distance and the GW uncertainty in amplitude, we can trivially solve for the chirp mass, \mathcal{M}_c using Eq. 1. The resulting probability distribution functions (pdf) are computed by randomly drawing points from the given distributions and computing the parameter of interest for each draw. The 95 percentiles in the \mathcal{M}_c are shown in the left panel of Figure 5 for J0651 (in black) and the high mass binary (in grey) as a function of inclination. The dashed lines (in black for J0651 and in grey for the high mass binary) are the real values. The decreasing medians of the chirp mass with inclination follows from the GW distributions in the amplitude that is shown in Figure 4 where the median \mathcal{A} is overestimated for $\iota = 5^\circ$ (in thin black lines) compared to that of $\iota = 90^\circ$ (in thick black lines). For a fixed distribution in distance the corresponding distribution of \mathcal{M}_c is therefore overestimated for $\iota = 5^\circ$ shown in the right panel of Figure 5 compared to that of $\iota = 90^\circ$. The 95 percentiles of the chirp masses for both J0651 and the high mass binary are affected by these overestimated medians of the amplitudes at lower inclinations which cause significant offsets of the \mathcal{M}_c from their respective real values as can be seen in the left panel of Figure 5. Thus at lower inclinations where the medians in the amplitude are overestimates, the 95 percentiles in the chirp mass can be interpreted as upper limits of the chirp mass.

In order to calculate reliable constraints in \mathcal{M}_c at these small inclinations we have to do full (Bayesian) data analyses that takes into account the physical priors and gives us a better estimate of the expected posterior distributions in the desired parameters. The 95 percentile in \mathcal{M}_c for both systems decrease as a function of inclination as is expected from the propagation of uncertainty where $\sigma_{\mathcal{M}_c} \propto \sigma_{\mathcal{A}}$. Thus, knowing distance from EM observation gives us an estimate of the chirp mass where the constraints are tighter for the higher inclination (eclipsing) systems.

3.2. Scenario 2: EM observations of single-lined spectroscopic binary

Some measurements are unique to EM observations such as the radial velocity K_1 , of one of the components (m_1) of the binary:

$$K_1 = \sin \iota \frac{m_2}{(m_1 + m_2)^{2/3}} \left(\frac{2\pi G}{P_{\text{orb}}} \right)^{1/3}, \quad (4)$$

which can be used to measure inclination. We adopt the convention from the optical studies of the binary sources where the primary mass, m_1 is the brighter object and the dimmer secondary mass, m_2 . Note that the inclination measurement from the GW data analysis, $\iota[\text{GW}]$ and from the radial velocity equation above i.e. $\iota[\text{RV}]$ are two independent measurements for the same system. We will show that these two are anti-correlated below in Sect. 3.2.3, yielding radial velocity measurements very useful.

3.2.1. Scenario 2a: EM data on m_1

Before looking at a real single-lined spectral binary we first consider the case that only the mass m_1 is known from the EM data. This is a viable scenario when determining K_1 is impossible and we may get an estimate of the primary mass from the photometry or the spectra. Assuming a double WD system, we take a uniform distribution for m_2 , which together with the given m_1 constrains the d . The estimates of distance with their corresponding 95 percentiles as a function of inclination are shown in Figure 6 for both the J0651 (in black) and

the high mass binary (in grey). The real value of distance is shown in the dashed (black) line. The offsets of the medians in the distance at low inclinations for both the binary systems can be explained in a similar way as in the previous sections, which is due to the over-estimated medians of \mathcal{A} at lower inclinations as shown in the left panel of Figure 4. Additionally, the significant discrepancy between the median distance for J0651 vs. the high mass binary (at $\iota \geq 40^\circ$) is again due to the over-estimated value of the \mathcal{M}_c for J0651 assuming a uniform distribution m_2 distribution. This is shown in the right panel of Figure 6 where the vertical dashed lines are their corresponding true values of the \mathcal{M}_c and the vertical solid lines are the medians of the corresponding distributions. The simulated distribution of \mathcal{M}_c from an EM measurement of m_1 with a Gaussian width in its uncertainty together with an assumed uniform distribution in the unknown m_2 results in an overestimated median of the \mathcal{M}_c for J0651 compared to that of the high mass binary. This propagates in overestimating the median d for J0651 at higher inclinations unlike for the high mass binary since its median \mathcal{M}_c is slightly underestimated. The flat priors on m_2 is affecting this and if we already know the secondary mass is low, we may take a distribution in m_2 weighted towards lower masses and that will affect the constraints obtained in the d . The constraints in the distance from Figure 6 can be compared with those in Figure 3 where there was no EM information on any of the masses: the upper limits on d for both J0651 and the high mass binary are constrained by a up to factor of ~ 4 better when m_1 is known for both binaries with 10% accuracy.

3.2.2. Scenario 2b: EM data on m_1 & K_1

In this case we consider EM measurements of a *single-lined spectroscopic* binary where resolving one of the masses of the binary spectroscopically typically provides measurements on the primary mass and its radial velocity. We assume an uncertainty in radial velocity amplitude of 10% corresponding to the typical accuracy of 10km/s found in the EM measurements (for e.g., Roelofs et al. 2006). Given m_1 and K_1 from the EM data and inclination from GW data $\iota[\text{GW}]$, we can numerically solve for m_2 via the K_1 formulation in Eq. 4. Assuming it is a WD, the m_2 is restricted to lie in $[0.1 - 1.4]M_\odot$. Then a fixed pair of $[\mathcal{A}, \iota[\text{GW}]]$ and the masses give us a distance. We calculate the resulting distributions in m_2 and the distance from the Gaussian distributions of m_1 and K_1 about their typical EM uncertainties and GW distributions in the inclination and amplitude. The 95 percentile in the secondary mass and the distance are shown in Figure 7 as a function of inclination for both J0651 (in black) and the high mass binary (in grey). Like in the scenarios discussed above, for the lowest inclinations, the over estimated FIM uncertainties of \mathcal{A} propagates into erroneous constraints on m_2 , and d . Thus, at lower inclinations we have to use Bayesian methods to get their accurate GW uncertainties. Observe that the 95 percentile in the m_2 and the distance roughly similar and large from $5^\circ < \iota < 45^\circ$. This is again due to the influence of the GW distributions in \mathcal{A} at the lower inclinations, which have uniform distributions resulting into over-estimated medians (see Figure 1). However, for $\iota > 45^\circ$ the uncertainties for both m_2 , and d decrease

with inclination and their medians stabilize at the true values. This is caused by the fact that at higher inclinations, the medians of GW amplitudes are close to the true values of the systems where the constraints on the GW parameters are also tighter with increasing inclination. Thus, the decreasing uncertainties in $\iota[\text{GW}]$ as a function of ι (see right panel of Figure 2) should result in the same behavior of σ_{m_2} via Eq. 4. Since distance is computed using these m_2 , the same behavior holds for the distance in the right panel.

3.2.3. Scenario 2c: EM data on m_1 , K_1 & d

Here the EM measurements of a *single-lined spectroscopic* binary in the previous subsection is complemented with a distance measurement from *Gaia* or from an estimate of the absolute magnitude. From the primary mass m_1 , distance and the amplitude we immediately get the secondary mass, m_2 . We will call this as the preliminary m_2 since this can be further improved by folding in the radial velocity measurement. As mentioned before the radial velocity measurement essentially provides an independent measurement of the inclination via Eq. 4. This can be seen in the following way: The GW parameters of the non-eclipsing J0651 are: \mathcal{A}_0 , $\iota_0 = 1.67 \times 10^{-22}, 45^\circ$ whose VCM uncertainties are: $\sigma_{\mathcal{A}}/\mathcal{A} = 0.231$, and $\sigma_\iota = 0.75$ rad respectively. We also take a fixed radial velocity, K_0 corresponding to m_1 , m_2 (listed in Table 1), and ι_0 . The 2-d Gaussian distribution from GW data with $1 - \sigma$ uncertainties for these parameters is shown in the left panel of Figure 8. For each randomly selected pair of $[\mathcal{A}, \cos \iota[\text{GW}]]$ and for a fixed m_1 , and d , we can solve for the m_2 from Eq. 1. Using this m_2 for that fixed m_1 and K_0 , we solve for $\iota[\text{RV}]$. For many points randomly picked in the $[\mathcal{A}, \cos \iota[\text{GW}]]$ space the computed $\iota[\text{RV}]$ are compared with the corresponding $\iota[\text{GW}]$ in the right panel. The inclinations measured in two ways roughly anti-correlate. However we know that values of $\iota[\text{RV}]$ that are different from $\iota[\text{GW}]$ cannot be true. Thus, constraining the inclination of the system in a small area around 45° along the diagonal line in the right panel also constrains m_2 and the amplitude. We make use of this in the case considered in this subsection. The preliminary m_2 and their 95 percentiles computed from EM data on m_1 , d , and the GW data on \mathcal{A} as a function of inclination is shown in Figure 9 in grey lines in the left panel for J0651. The same for the high mass binary is also shown in the right panel in grey lines. From this m_2 , given m_1 , and $\iota[\text{GW}]$, the radial velocity, K_{GW} is computed which is compared with the K_1 from the EM data. Since the EM measured K_1 is more precise, we keep the subset of those K_{GW} and the respective $\iota[\text{GW}]$ weighted with a probability distribution function of the K_1 given by:

$$\mathcal{P}_i = \frac{1}{\sqrt{2\pi} \sigma_{K_1}} \exp\left(\frac{-0.5 (K_{1,i}[\text{GW}] - K_1)^2}{\sigma_{K_1}^2}\right) dK_1. \quad (5)$$

The final reduced 95 percentiles in m_2 are shown in black lines for J0651 in left panel, and the same is shown for the high mass binary in the right panel. Observe that the uncertainties in m_2 calculated in this way for lower inclinations is the similar to those at the higher inclinations. Thus, the advantage of folding in K_1 measurement is *especially* useful for lower inclination systems with S/N

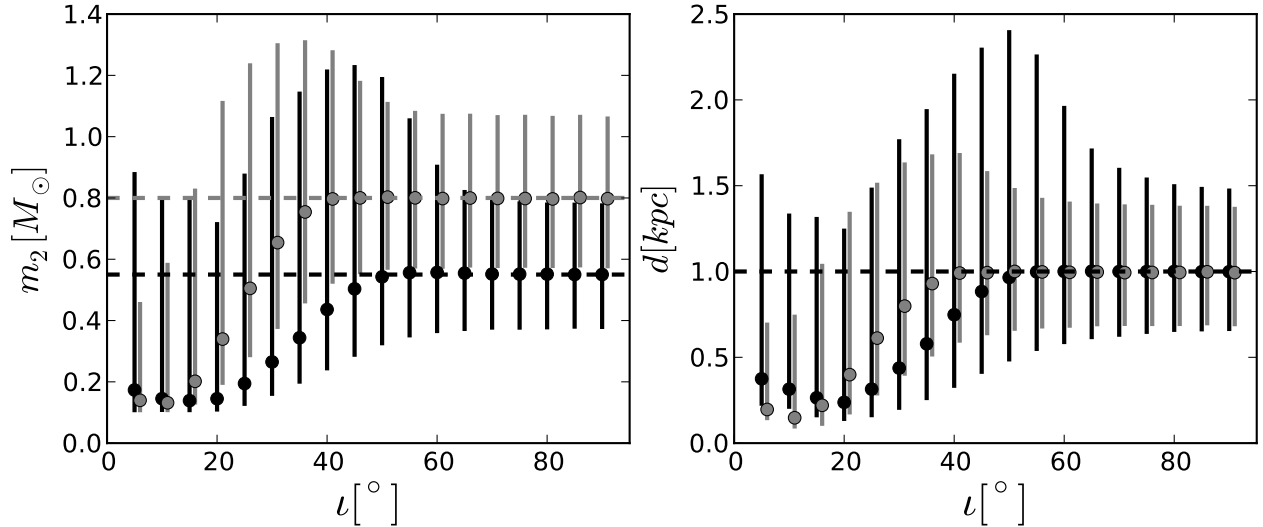


FIG. 7.— *Scenario 2b*: Constraints on the secondary mass and distance from combining *single spectroscopic* EM data: m_1 , and K_1 with GW data on \mathcal{A} , ι for J0651 (black) and the high mass binary (in grey).

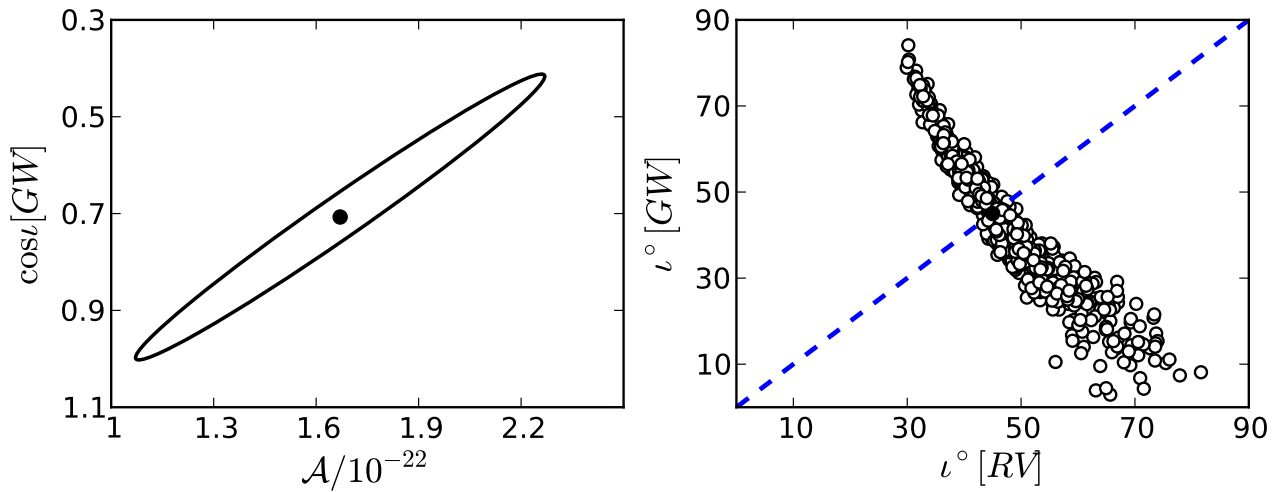


FIG. 8.— Relation between inclination from GW observation vs. that from EM observations. *Left* 2-d error ellipse from the GW data analysis in amplitude and $\cos \iota$ for J0651 with $\iota = 45^\circ$. *Right*: Relation between inclination from the left panel and inclination from Eq. 4.

~ 10 , where large GW uncertainties \mathcal{A} influence the constraints of the physical parameters in question. Furthermore, the constraints in m_2 can also be compared with the previous case in Figure 7 where we find that for the single-lined spectroscopic binary, knowing its distance to 10% significantly improves knowledge of the secondary mass at lower inclinations.

The key point in Scenarios 2b and 2c is that not all the $[\mathcal{A}, \iota[\text{GW}]]$ pairs are consistent with the EM observations. Therefore both constraints on the GW data and other parameters also constrain the GW error ellipses. The $2-\sigma$ uncertainties in the GW amplitude and GW inclination for these scenarios are shown in the Appendix.

3.3. Scenario 3: EM data on m_1 , K_1 , m_2 & K_2

In this section we consider EM observations of a *double-lined spectroscopic* binary which translates to a set of measurements in the mass and radial velocity for each of the components: m_1 , K_1 , and m_2 , K_2 . Given the two masses and GW measurement on the amplitude we can immediately compute a preliminary distance. Additionally, we can also derive two sets of inclinations inde-

pendently from the individual radial velocities and the masses, ι_{K_1}, ι_{K_2} from Eq. 4. These inclinations can be compared with the one measured from GW data, $\iota[\text{GW}]$. At lower inclinations, large uncertainties in $\iota[\text{GW}]$ essentially imply that those systems' inclinations are undetermined and this also affects the amplitude due to the strong correlation between them. Thus, the independent estimates of ι_{K_1}, ι_{K_2} from the EM data can be useful in constraining the GW amplitude. This reduced amplitude will further constrain the distance which is shown in the third panel in Figure 10. In the figure both the observed K_1, K_2 are shown in the left panel in thick and thin black lines respectively. The inclination and the distance given the GW amplitude and both the masses are shown in grey line in the middle and right panels respectively. Both the inclination and distance derived from K_1 and K_2 are plotted in thick and thin black lines respectively. Observe that a 10% fractional error in each K_1 and K_2 translate into similar uncertainties of the distance and thus in the following figures we show the constraints from using K_1 data only. The constrained distances estimated in this way as a function of inclination is shown in

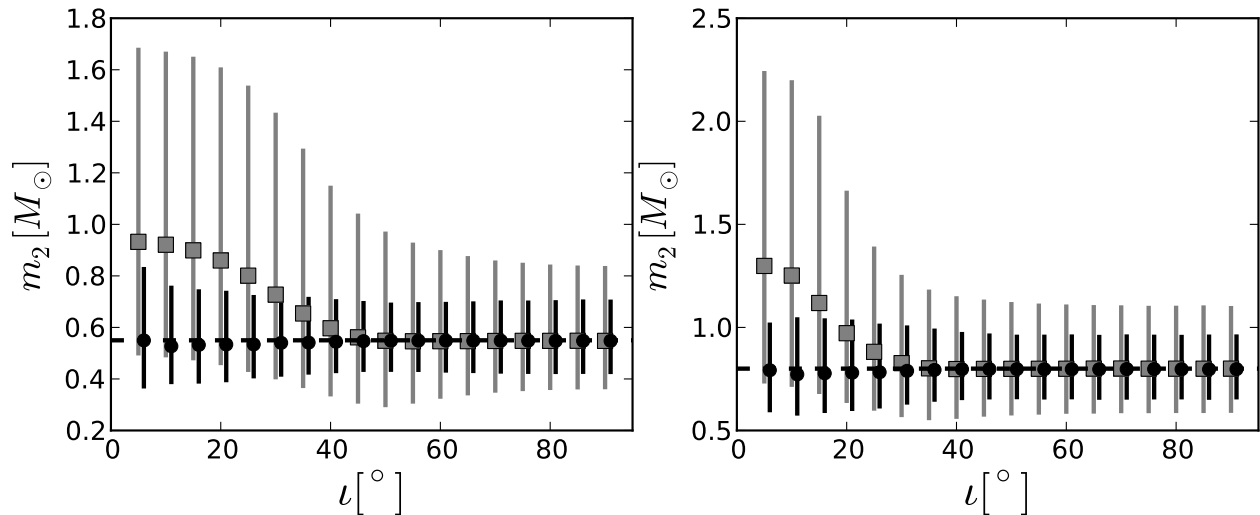


FIG. 9.— *Scenario 2c*: Same scenario as in Figure 7 with an additional EM measurement on the distance. Left: $2 - \sigma$ uncertainties for the secondary mass for J0651 where the grey colored lines are constraints from EM information on m_1 , d and GW \mathcal{A} . These reduce to the tighter constraints shown in black lines when EM data on K_1 is also used (see text). The dashed line in red is the real value of m_2 . Right: Same for the high mass binary.

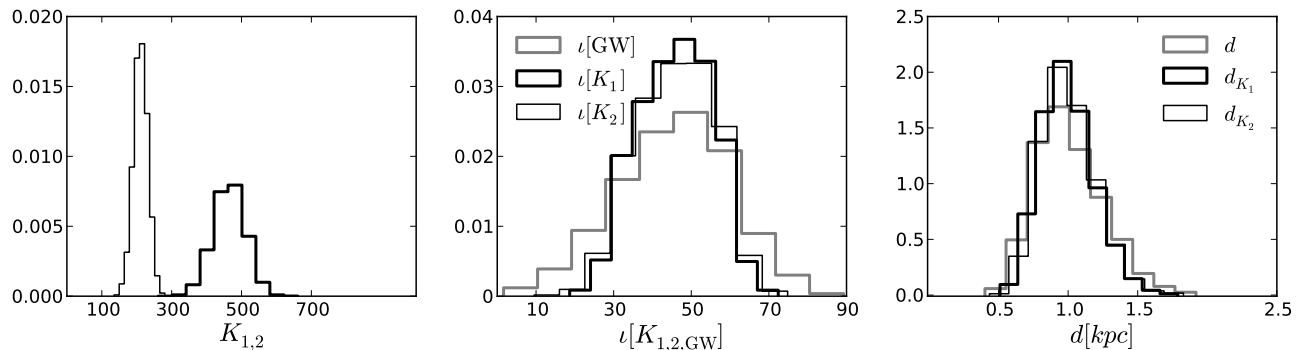


FIG. 10.— *Scenario 3*: Left: Distributions of the radial velocities from EM data for J0651 masses with the binary orientated at $\iota = 45^\circ$. Middle: Given EM data on m_1, m_2 , and the corresponding K_1, K_2 , the inclinations are calculate using Eq. 4 which is compared with inclination from GW data. Right: Constraints on the distance obtained solving Eq. 1 with: EM data on m_1, K_1, m_2, K_2 and GW data on \mathcal{A}, ι .

Figure 11 for J0651 in left panel (also in black) and for the high mass binary in the right panel (in black). The grey lines in both the panels are the 95 percentiles in d using only the masses from the EM data and the GW amplitude. Observe that at lower inclinations knowing masses and a radial velocity can improve the constraint in distances significantly. The uncertainties are smaller for J0651 at lowest inclinations because the relative 10% uncertainties in the K_1 have lower absolute uncertainties that propagate into the uncertainties of the distance.

Note that typically in practice EM data provides measurements of both the masses and only one of the radial velocities with $\sim 10\%$ precision. From the radial velocity formulation we have the relation: relation $m_1/m_2 = K_2/K_1$ which can be used to compute the remaining K_i . This provides a consistency check between EM and GW data. The EM data can be used to derive inclination measured from the radial velocities, $\iota[\text{RV}]$ which can be verified against the $\iota[\text{GW}]$ as shown in the middle panel in Figure 10.

4. CONCLUSIONS

We have quantified the possible constraints/improvements in the physical parameters

of the white-dwarf (WD) binaries that are observable by the eLISA detector in the future when combined with the EM data. We do this for the binary parameters that are astrophysically interesting (masses and distance). For the GW observations from eLISA, we calculate the source's variance-covariance matrix using the Fisher methods where the Galactic binary source is described by seven parameters (or eight if \dot{f} is measurable). We have taken J0651 and a higher mass binary in our analyses where J0651 is a *verification* source for eLISA. We consider various possible cases depending on the availability of the EM measurements and combine those with GW uncertainties in the amplitude and inclination in order to solve for the unknown parameters as a function of inclinations for both J0651 and the high mass binary. For clarity we list all the cases below:

1. *GW data only*: Assuming a double white-dwarf system this scenario somewhat constrains the distance.
2. *Scenario 1*: GW data + distance d : This scenario constrains the chirp mass \mathcal{M}_c .
3. *Scenario 2a*: GW data + primary mass m_1 : This

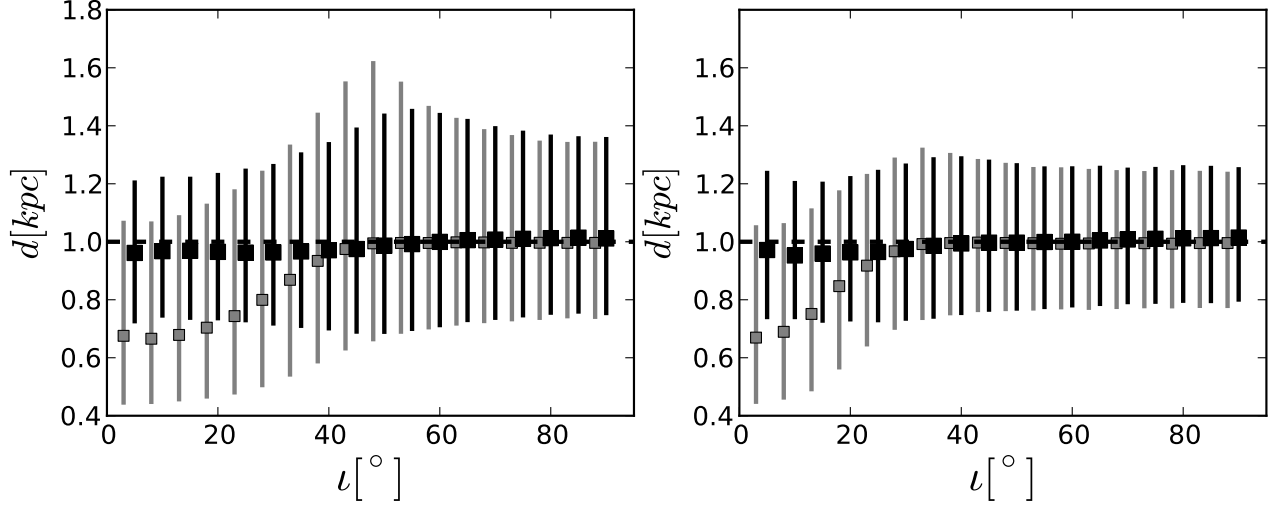


FIG. 11.— *Scenario 3*: Same as in Figure 10 but for all inclinations for J0651 in left panel and the for the high mass binary in right panel. The constraints in black lines are from using $\iota[K_1]$ and the constraints in grey are from using $\iota[GW]$. The dashed line (in black) is the real values of the d .

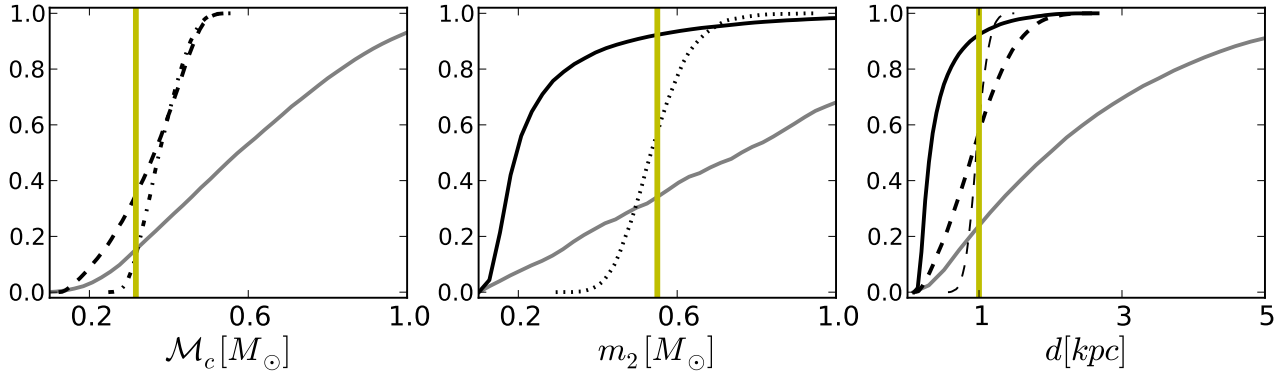


FIG. 12.— Comparison of normalized CDFs in \mathcal{M}_c , m_2 , and d for all the scenarios above for J0651 with $\iota = 25^\circ$. The vertical lines (in yellow) in all the panels are the true values of the parameters. The solid curves in grey are CDFs for the parameters when only GW data is available. Curves in dash-dotted lines are constraints for *Scenario 1* (known distance d), dashed curves are for *Scenario 2a* (known primary mass m_1), solid curves are for *Scenario 2b* (known primary mass m_1 and radial velocity K_1), dotted curves are for *Scenario 2c* (known m_1 , K_1 and d) and thin-dashed lines are for *Scenario 3* (known both masses m_1, m_2 and radial velocities K_1, K_2).

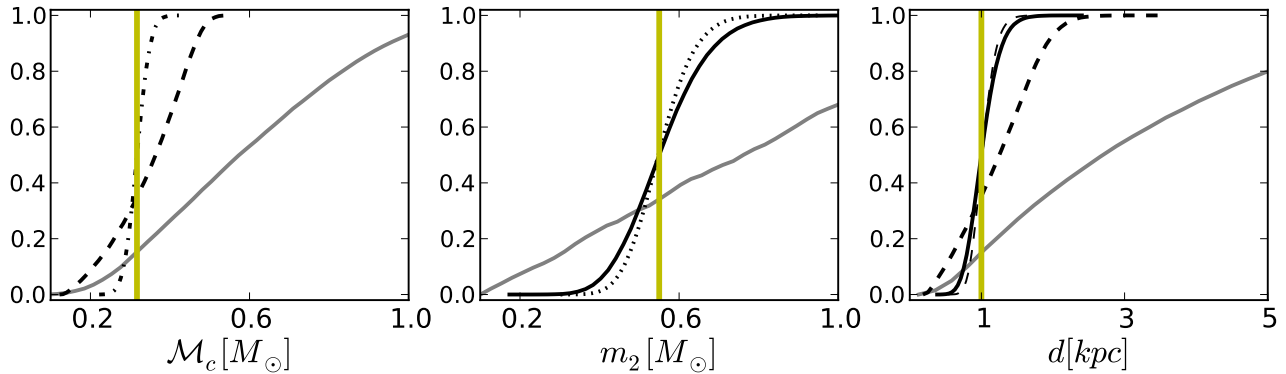


FIG. 13.— Same as in Figure 12, for $\iota = 85^\circ$.

scenario constrains the chirp mass and the distance.

4. *Scenario 2b*: GW data + single-lined spectroscopic binary i.e. m_1, K_1 : This scenario constrains the secondary mass m_2 and the distance.
5. *Scenario 2c*: GW data + single-lined spectroscopic binary + d : This scenario also constrains the secondary mass m_2 .
6. *Scenario 3*: GW data + double-lined spectroscopic binary i.e. m_1, K_1 and m_2, K_2 : This scenario constrains the distance.

All the $1 - \sigma$ EM accuracies are taken to be 10% of the real/measured values which is inspired by several EM observations. We compare below the constraints in the physical parameters of interest: secondary mass m_2 , chirp mass \mathcal{M}_c and the distance d as a function of the scenarios depending on the EM information available. Since the GW parameter uncertainties are significantly different for a low inclination (face-on) orientation than for a high inclination (edge-on) orientation, we do the comparison for a non-eclipsing J0651 with $\iota = 25^\circ$ and an almost eclipsing J0651 with $\iota = 85^\circ$ in Figures 12 and 13 respectively and conclude the following:

1. *Constraints on chirp mass, \mathcal{M}_c* : In the left panels of Figures 12 and 13, EM data on d constrains the 95 percentile of the system's chirp mass (dash-dotted line) to $0.38^{+0.11}_{-0.09}M_\odot$ and $0.32^{+0.05}_{-0.05}M_\odot$ for face-on and eclipsing J0651 respectively. EM data on m_1 constrains the \mathcal{M}_c (in thick-dashed line) to $0.36^{+0.13}_{-0.21}M_\odot$ which does not depend on the inclination. The normalized cumulative distributions (CDF) of the constraints on the distance are compared to that from GW data only which is shown in the grey line in both panels.

2. *Constraints on secondary mass, m_2* : In the middle panels of Figures 12 and 13, EM data on the m_1, K_1 constrain the 95 percentile of secondary mass, m_2 to $0.19^{+0.69}_{-0.07}M_\odot$ and $0.55^{+0.23}_{-0.18}M_\odot$ for face-on and eclipsing J0651 respectively (shown in solid lines). The same set of data complemented with the distance further constrain the 95 percentile in m_2 with $0.55^{+0.18}_{-0.13}M_\odot$ and $0.55^{+0.16}_{-0.13}M_\odot$ for face-on and eclipsing J0651 respectively (shown in dotted lines). For comparison, the CDF of m_2 using only the GW data is shown in grey.
3. *Constraints on distance, d* : In the right panels, of Figure 12 and 13, EM data on m_1 constrains the distance to $0.91^{+0.98}_{-0.69}$ kpc and $1.25^{+0.95}_{-0.95}$ kpc for face-on and eclipsing J0651 respectively (in thick-dashed lines). EM data on the m_1, K_1 constrain the 95 percentile in d with $0.32^{+1.17}_{-0.16}$ kpc and with $0.99^{+0.49}_{-0.35}$ kpc accuracy for face-on and eclipsing J0651 respectively (in solid lines). EM data on m_1, m_2, K_1 and K_2 constrain the 95 percentile in d to $0.96^{+0.29}_{-0.24}$ kpc and $1.01^{+0.35}_{-0.26}$ kpc for face-on and eclipsing J0651 respectively (in thin-dashed line). For comparison, the CDF of d using only the GW data and the assumption that the masses are WDs is shown in grey.

Thus, knowing distance and/or radial velocity of the primary component can significantly improve our knowledge of the binary system. These constraints change as a function of inclination of the binary that is shown in previous sections. In a forthcoming paper we will address the effect on these improvements by including the (possible) EM measurement of rate of change of the orbital period.

This work was supported by funding from FOM. We are very grateful to Michele Vallisneri for providing support with the *Synthetic LISA* and *Lisasolve* softwares.

REFERENCES

- Amaro-Seoane, P., Aoudia, S., Babak, S., et al. 2013, GW Notes, Vol. 6, p. 4-110, 6, 4
- Bailer-Jones, C. A. L. 2009, in IAU Symposium, Vol. 254, IAU Symposium, ed. J. Andersen, Nordströara, B. m, & J. Bland-Hawthorn, 475–482
- Brown, W. R., Kilic, M., Hermes, J. J., et al. 2011, ApJ, 737, L23
- Cutler, C. 1998, Phys. Rev. D, 57, 7089
- de Bruijne, J. H. J. 2012, Ap&SS, 341, 31
- Hermes, J. J., Kilic, M., Brown, W. R., et al. 2012, ApJ, 757, L21
- Nelemans, G. 2009, Classical and Quantum Gravity, 26, 094030
- Nelemans, G., Yungelson, L. R., & Portegies Zwart, S. F. 2001, A&A, 375, 890
- Nissanke, S., Vallisneri, M., Nelemans, G., & Prince, T. A. 2012, ApJ, 758, 131
- Peters, P. C., & Mathews, J. 1963, Physical Review, 131, 435
- Rodriguez, C. L., Farr, B., Farr, W. M., & Mandel, I. 2013, Phys. Rev. D, 88, 084013
- Roelofs, G. H. A., Groot, P. J., Nelemans, G., Marsh, T. R., & Steeghs, D. 2006, MNRAS, 371, 1231
- Roelofs, G. H. A., Rau, A., Marsh, T. R., et al. 2010, ApJ, 711, L138
- Shah, S., Nelemans, G., & van der Sluys, M. 2013, A&A, 553, A82
- Shah, S., van der Sluys, M., & Nelemans, G. 2012, A&A, 544, A153
- Vallisneri, M. 2008, Phys. Rev. D, 77, 042001
- Verbeek, K., Groot, P. J., Nelemans, G., et al. 2013, MNRAS, 434, 2727

APPENDIX

VARIANCE-COVARIANCE MATRIXES OF J0651

We have listed the VCM matrices for the J0651 system with eclipsing and non-eclipsing configurations in our analysis. There are 7 parameters that describe them which are listed in the first row of the matrices below and for each binary, the values are listed in the row with θ_i . The diagonal elements are the absolute uncertainties in each the 7 parameters and the off-diagonal elements are the normalized correlations, i.e. $c_{ii} = \sqrt{C_{ii}} \equiv \sigma_i$, $c_{ij} = \frac{C_{ij}}{\sqrt{C_{ii}C_{jj}}}$. The strong correlations between parameters (i.e. whose magnitudes are ≥ 0.9) are marked in bold in the VCMs below. These correlations have been explained in Paper I.

VCM 1: Eclipsing J0651 ($\iota = 5^\circ$), S/N = 10.5.

θ_i	\mathcal{A}	ϕ_0	$\cos \iota$	f	ψ	$\sin \beta$	λ
θ_i	1.67×10^{-22}	π	0.007	2.61×10^{-3}	$\pi/2$	-0.08	2.10
\mathcal{A}	0.08×10^{-23}	-0.0	0.0	0.01	0.02	0.03	-0.06
ϕ_0		0.907	-0.01	-0.91	0.01	0.11	0.08
$\cos \iota$			0.172	0.01	-0.01	0.07	-0.33
f				2.982×10^{-10}	-0.01	-0.08	-0.15
ψ					0.035	-0.02	0.05
$\sin \beta$						0.059	0.08
λ							0.017

VCM 2: Not-eclipsing J0651 ($\iota = 45^\circ$), S/N = 24.

θ_i	\mathcal{A}	ϕ_0	$\cos \iota$	f	ψ	$\sin \beta$	λ
θ_i	1.67×10^{-23}	π	0.707	2.61×10^{-3}	$\pi/2$	-0.08	2.10
\mathcal{A}	3.86×10^{-23}	0.03	-0.98	-0.02	0.03	-0.13	0.35
ϕ_0		0.739	-0.03	-0.19	0.16	0.15	0.10
$\cos \iota$			0.19	0.02	-0.01	0.13	-0.36
f				1.688×10^{-9}	-0.98	-0.06	-0.21
ψ					0.36	0.13	0.07
$\sin \beta$						0.031	-0.13
λ							0.009

CONSTRAINTS IN \mathcal{A} AND ι OF J0651

Figure 14 shows how the error ellipses of amplitude and inclination from GW observations reduce using EM observations for the different scenarios that we have described in Sects. 1 and 2. Knowing one of the masses (Scenario 2a) from the EM does not constrain the $[\mathcal{A}, \iota]$ any more than the GW data alone. In other words the m_2 and d are free parameters to satisfy the amplitude. The 95 percentiles in the amplitude are shown in grey in the figure which are the same as the case where we have GW data only. In fact these constraints in the amplitude decrease as a function of inclination as expected from the GW measurements (see Figure 2). Adding an EM measurement of the measured mass's radial velocity (Scenario 2b) can constrain the $[\mathcal{A}, \iota]$ slightly or significantly depending on inclination of the system which are shown in thick black lines. Finally complementing the mass and radial velocity of the brighter companion with the distance to the binary (Scenario 2c) significantly constraints the $[\mathcal{A}, \iota]$ which is strongest for the lower inclinations as shown in the figure in thin black lines. Observe that EM information provide strongest improvements for low inclination systems where GW uncertainties in the amplitude and the inclination are very large.

THE DISTRIBUTION OF \mathcal{A} AND ι AT LOWER INCLINATIONS

Here we show that while Fisher method gives an estimate on the parameter uncertainties and correlation between them without following the posterior in detail, it gives a reasonable estimate of the above quantities as long as the priors in the parameters are rectangular (i.e. not Gaussian) and are large enough to preserve the overall orientation of the posterior. We compute an estimate of the likelihood with a simple χ^2 procedure on a 2D parameter distribution of \mathcal{A}_i and $\cos \iota_j$, where the $\chi^2 = (1/(N-1)) \sum_{t=0, N} (h_0(t) - (h[i, j](t) + n(t)))^2$, h_0 = true signal, $h[i, j]$ = signal at a grid point and n is a noise realisation, N = total time samples. For an evenly placed parameters in a 10×10 grid, we take the average χ^2 computed for 10 different noise realisations. Figure 15 shows the colored contours of 2D χ^2 distribution for the case of $\iota = 65^\circ$ (in the left-panel) where the Fisher uncertainties are well within the physically allowed bounds. The over-plotted contour in thick solid line is $1 - \sigma$ uncertainty ellipse computed from Fisher matrix about the true values of \mathcal{A} and $\cos \iota$ labelled with the white circle. This just shows that the χ^2 distribution follows the shape and the slope of the Fisher distribution roughly, but not exactly as expected. The same is shown for $\iota = 10^\circ$ in the right-panel where the uncertainties hit the physical bounds and both the methods show a sharp cut-off at $\cos \iota = 1$. Here we see that again the Fisher uncertainties and correlation roughly follow that of the χ^2 , but with truncations at the boundaries. The deviation in the top-right is discussed in Shah et al. (2012). It was argued that although the results of Fisher-based uncertainties imply that the $\iota = 5^\circ$ system is very similar to $\iota = 90^\circ$, this is unlikely because of the anti-correlation between \mathcal{A} and $\cos \iota$ at high inclinations. At $\iota \gtrsim 45^\circ$ correlation between \mathcal{A} and $\cos \iota$ decreases ι

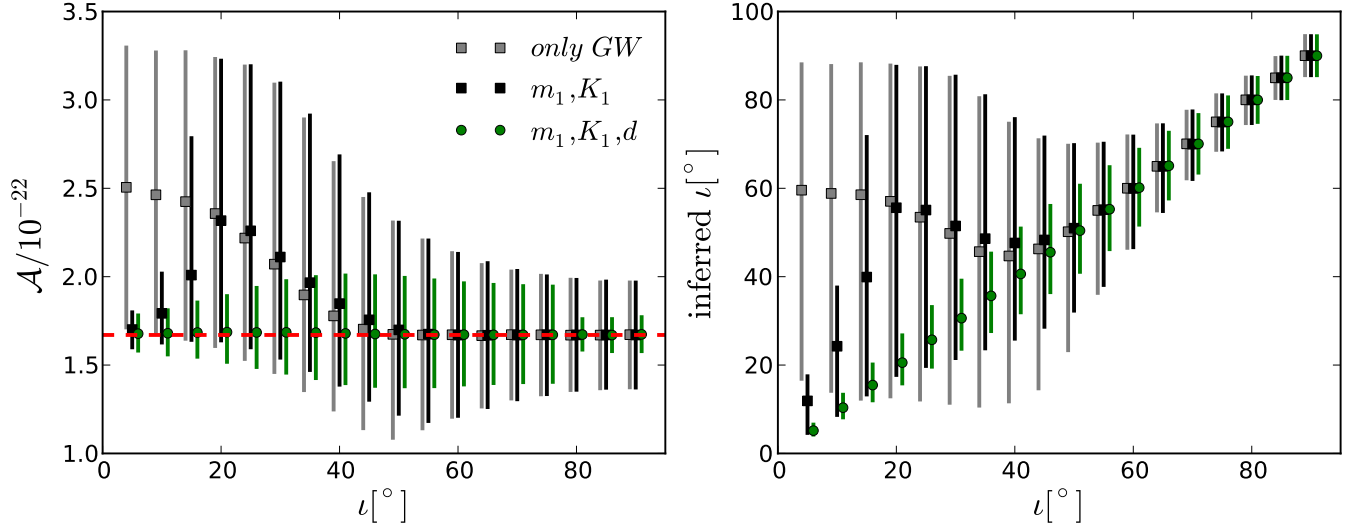


FIG. 14.— 95 percentiles in the GW amplitude as a function of inclination for various sets of EM information as labeled. The real value for the amplitude is shown in black dashed-line.

and the high accuracy in the inclination itself actually suffices to distinguish the higher inclination systems. Thus we expect that that χ^2 deviates from the Fisher estimate towards the top-right region of the Figure 15 in the right-panel.

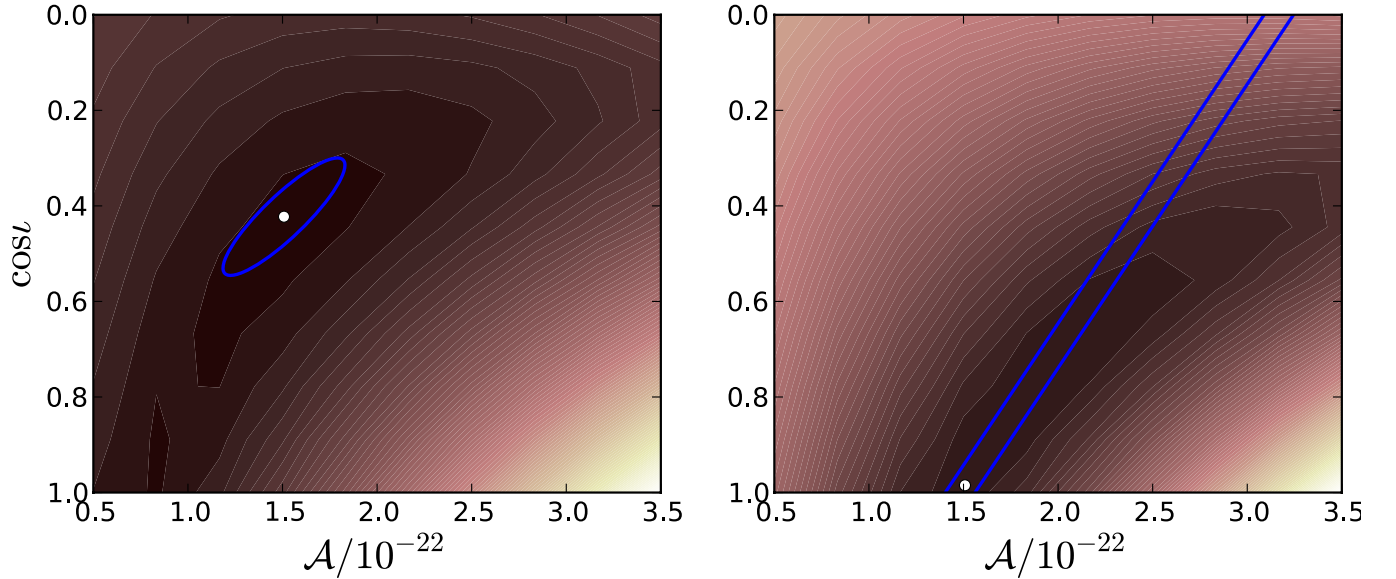


FIG. 15.— Filled contour plot of the 2D χ^2 averaged over 10 noise realisations for an evenly distributed grid of \mathcal{A} and $\cos \iota$ compared with the $1 - \sigma$ error ellipse (shown in thick solid line) from Fisher matrix $\iota = 65^\circ$ in the left-panel and $\iota = 10^\circ$ in the right-panel. The χ^2 values are represented by the darker to lighter colors corresponding to lower to higher values in χ^2 .